have been proposed by Friedel[4] *et al.* and Anderson.[5] They are referred to as virtual energy states and are created by transition element impurities. It is proposed that these states are responsible for the stationary peak in the absorption curve at 300 nm. The position of the virtual energy states below and above the Fermi level could shift. However, the energy difference between the Fermi surface and the occupied or unoccupied virtual states should be independent of the Fermi energy position. Similar studies on *Au*Ni and *Au*Pd alloys[6,7] reveal the formation of new absorption structures due to impurity states in the near infrared. Computations[8] indicate energy ground-state solutions for impurity states of *Cu*Ni of the order of 0.1–0.2 Ry. Small modifications in the atomic integrals can change the impurity potential by similar accounts. Therefore, the theory gives no accurate results for our alloys.

The concept of impurity states could explain some anomalies in the optical absorption of *Cu*Ni alloys. The experiments[3] showed no noticeable change in the position of the main absorption edge near 600 nm. This was explained as due to the formation of virtual energy states. The secondary absorption structure at 300 nm seemed to move with increasing concentrations of nickel to lower wavelength by about 20 nm. From our present studies we would conclude that this shift is due to virtual energy states with optical absorptions near 300 nm. Their absorption peak may be slightly concentration-dependent and could move with increasing nickel concentration to lower wavelengths. This peak would be superimposed on the secondary absorption structure of copper. We intend to study this effect in detail.

ACKNOWLEDGMENTS

The authors are grateful to the National Science Foundation for grants which made this work possible and to Professor C. McCain for his assistance in construction of the experimental system.

[6] F. Abeles in *Optical Properties and Electronic Structure of Metals and Alloys*, edited by F. Abeles (North-Holland Publishing Co., Amsterdam, 1966), p. 553.
[7] B. Caroli, Phys. Kondensierten Materie **1**, 346 (1963).
[8] J. B. Sokoloff, Phys. Rev. **161**, 540 (1967).

PHYSICAL REVIEW VOLUME 167, NUMBER 3 15 MARCH 1968

Band Structure, Fermi Surface, and Knight Shift of Indium Metal*

G. D. GASPARI† AND T. P. DAS
Department of Physics, University of California, Riverside, California
(Received 28 October 1965; revised manuscript received 16 October 1967)

The orthogonalized-plane-wave (OPW) method has been applied to calculate the energy levels at several symmetry points in the Brillouin zone in indium metal. The calculated energy values were utilized to obtain parameters for the pseudopotential interpolation scheme. Using these parameters, a number of dimensions of the second- and third-zone Fermi surface were calculated and compared with experimental results from de Haas–van Alphen and magnetoacoustic measurements. The calculated Fermi surface qualitatively resembled that expected from the nearly-free-electron approximation. There were, however, differences in detail which brought the theoretical results into better agreement with experiment. The effect of spin-orbit interaction on the band structure was found to be small. The conduction-electron wave functions were calculated at a number of points on the Fermi surface using the OPW method. These wave functions were used to calculate the isotropic Knight shift, which was found to be 0.81%, in good agreement with experiment.

I. INTRODUCTION

IN recent years, the rapid development of experimental techniques for the study of the shape and dimensions of the Fermi surface has led to the accumulation of a considerable body of such data in a number of metals.[1] Concurrently, the development of theoretical methods[2] for computing energy bands has permitted a fairly detailed comparison[3] between the features of the Fermi surface determined experimentally and theoretically. Since these features require for their interpretation only a knowledge of the energy bands, little attention has been paid to the calculation of wave functions in solids. With the advent of nuclear- and electron-resonance techniques, several additional properties are now available which require for their interpretation a detailed knowledge of the wave functions. Examples of such properties are isotropic and anisotropic Knight shifts, nuclear quadrupole interaction, electronic g factors, and relaxation times for nuclear and electron spin resonance.

* Supported by the National Science Foundation.
† Present address: Department of Physics, University of California, Santa Cruz, Calif.
[1] W. A. Harrison and M. B. Webb, *International Conference on the Fermi Surface of Metals* (John Wiley & Sons, Inc., New York, 1960).
[2] J. Callaway, *Energy Band Theory* (Academic Press Inc., New York, 1964).
[3] W. A. Harrison, Phys. Rev. **118**, 1190 (1960).

From the study of the properties of molecules and atoms,[4] it appears that energy by itself is not a satisfactory criterion for determining the accuracy of wave functions since energy is a quantity which depends on all of configuration space. Other electromagnetic properties that depend on a specific region of configuration space allow a more severe test of the theoretical model and resulting wave functions. It would therefore be interesting to investigate for metals how well one could, starting from a particular model, interpret both the properties that depend explicitly on energy bands and the properties that require in addition a knowledge of the wave function. Indium is a particularly suitable metal for such an investigation because of the wealth of data of both kinds which are currently available for it.[5–8]

The choice and evaluation of the crystal potential are described in Sec. II. In Sec. III the procedure for calculation of the energy by the orthogonalized-plane-wave (OPW) method is described. The results of the OPW calculation at symmetry points are used to obtain pseudopotential parameters for interpolation of the energy bands. The resulting band structure is compared with experimental data in Sec. IV. Spin-orbit effects are discussed in Sec. V. The calculation of the Knight shift and a comparison between its theoretical and experimental values are presented in Sec. VI, and concluding remarks are given in Sec. VII.

II. POTENTIAL FOR THE CONDUCTION ELECTRON

The crystal structure of indium metal can be described alternatively as either body-centered tetragonal (bct) with $c/a=1.532$ or as a face-centered tetragonal lattice[5] (fct) with $c/a=1.08$. The Brillouin zone (BZ) is obtained in the usual manner and is shown in Fig. 1 together with some of the important symmetry points.[9]

The potential for the conduction electrons can be written as

$$V(\mathbf{r})=\sum_{\mu} V(\mathbf{r}-\mathbf{R}_{\mu}), \tag{1}$$

where the summation is over all lattice sites. We make the usual approximation of a spherical Wigner-Seitz cell[2] [radius $r_s=3.4788$ atomic units (a.u.)] and a central potential

$$V(\mathbf{r})=-2Z(r)/r \tag{2}$$

within each cell (in rydbergs). In computing $Z(r)$ we separate the various contributions along the lines of Heine.[10]

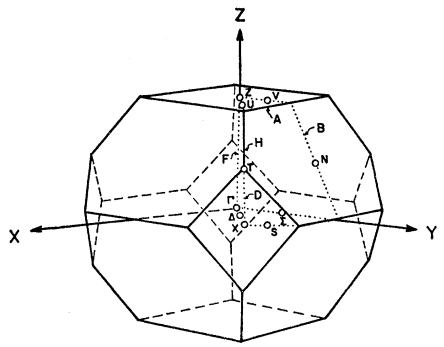

FIG. 1. Brillouin zone for indium with symmetry points and lines indicated.

$Z_1(r)$: Coulomb Potential due to the Nuclei and Core Electrons

Since there is little overlap between core electrons, the contributors to $Z_1(r)$ will be the nuclear charge of 49 and the surrounding core electrons in closed shells $1s^2$ through $4d^{10}$. For the latter, Herman and Skillman's Hartree-Fock-Slater wave functions[11] for indium atom were used. The screening effect of the conduction electrons was accounted for by using core wave functions for the neutral atom rather than In^{+++}.

$Z_2(r)$: Exchange Potential between Core and Conduction Electrons

For the core-conduction exchange we have adopted the prescription of Robinson, Bassani, Knox, and Schrieffer[12] who have tried to incorporate Coulomb correlation within the framework of the Slater exchange approximation, and have derived a modified expression for the Slater potential

$$V_{\text{Sc ex}}=-[(3/8\pi)\rho(r)F^3(\alpha)]^{1/3}, \tag{3}$$

where $F(\alpha)$ is charge-density-dependent and is given by

$$F(\alpha)=1-\tfrac{4}{3}\alpha\tan^{-1}(2/\alpha)+\tfrac{1}{2}\alpha^2\ln(1+4/\alpha^2) -\tfrac{1}{6}\alpha^2[1-\tfrac{1}{4}\alpha^2\ln(1+4/\alpha^2)], \tag{4}$$

with

$$\alpha=0.646/[\rho(r)]^{1/6}.$$

The correction factor $F(\alpha)$ has the effect of reducing the unscreened exchange potential at all distances but this reduction becomes most severe in the low-density region. This is important because the unscreened Slater potential is known to overexaggerate exchange effects

[4] T. P. Das and R. Bersohn, Phys. Rev. **115**, 897 (1959).
[5] J. A. Rayne and B. S. Chandrasekhar, Phys. Rev. **125**, 1952 (1962); J. A. Rayne, *ibid.* **129**, 652 (1963).
[6] G. B. Brandt and J. A. Rayne, Phys. Rev. **132**, 1512 (1963); Phys. Letters **12**, 87 (1964).
[7] P. R. Torgeson and R. G. Barnes, Phys. Rev. Letters **9**, 255 (1962).
[8] J. E. Adams and L. Berry and R. R. Hewitt, Phys. Rev. **143**, 164 (1966); T. T. Taylor and R. R. Hewitt, *ibid.* **125**, 524 (1962).
[9] G. F. Koster, in *Solid State Physics*, edited by F. Seitz and D. Turnbull (Academic Press Inc., New York, 1955), Vol. 5.
[10] V. Heine, Proc. Roy. Soc. (London) **A240**, 340 (1957); **A240**, 354 (1957); **A240**, 361 (1957).
[11] F. Herman and S. Skillman, *Atomic Structure Calculation* (Prentice-Hall, Inc., Englewood Cliffs, N. J., 1963).
[12] J. E. Robinson, F. Bassani, R. S. Knox, and J. R. Schrieffer, Phys. Rev. Letters **9**, 215 (1962).

TABLE I. The crystal potential.

X[a]	Z_1[b]	Z_2[c]	Z_3[d]	Z_5[e]	Z_T[f]
0.01	48.3259	0.1136	−0.0031	0.0002	48.4365
0.10	43.1064	0.5406	−0.0313	0.0019	43.6175
0.20	38.7152	0.6163	−0.0626	0.0038	39.2726
0.30	35.0453	0.7372	−0.0939	0.0057	35.6943
0.46	30.3298	0.8410	−0.1439	0.0087	31.0356
0.62	26.6532	0.8458	−0.1939	0.0117	27.3169
0.78	23.6110	0.8309	−0.2439	0.0148	24.2128
1.02	19.8906	0.8989	−0.3187	0.0193	20.4901
1.26	17.0417	0.9358	−0.3933	0.0238	17.6081
1.50	14.8890	0.9072	−0.4677	0.0284	15.3563
1.98	11.8309	0.6972	−0.6157	0.0375	11.9498
2.46	9.5680	0.5902	−0.7623	0.0465	9.4424
2.94	7.7617	0.6316	−0.9072	0.0556	7.5416
3.42	6.3622	0.6838	−1.0501	0.0647	6.0606
4.06	5.0562	0.7225	−1.2368	0.0768	4.6187
4.70	4.2384	0.6518	−1.4185	0.0889	3.5606
5.34	3.7434	0.5010	−1.5943	0.1010	2.7511
5.98	3.4480	0.3726	−1.7636	0.1131	2.1700
6.94	3.2126	0.2278	−2.0032	0.1312	1.5684
8.22	3.0818	0.1125	−2.2922	0.1554	1.0574
9.50	3.0336	0.0549	−2.5405	0.1796	0.7276
10.78	3.0156	0.0271	−2.7416	0.2038	0.5050
12.06	3.0089	0.0137	−2.8892	0.2280	0.3614
13.98	3.0060	0.0051	−2.9966	0.1801	0.1946
15.26	3.0000	0.0027	−3.0000	0.0926	0.0925

[a] $X=r/\mu=r/0.241942$.
[b] Z_1 is the Coulomb potential due to ion cores.
[c] Z_2 is the screened Slater exchange potential between ion cores and conduction electrons.
[d] Z_3 is the Coulomb potential due to conduction electrons.
[e] Z_5 is the correction due to deviation from spherical symmetry.
[f] Z_T is the total crystal potential.

in the low-density region[13] leading to a total potential with a rather long tail.

$Z_3(r)$: Coulomb Potential between Conduction Electrons

In calculating the potential due to the conduction electrons, we have assumed a uniform distribution of three electrons in each Wigner-Seitz sphere. The potential resulting from such a distribution is

$$\begin{aligned} Z_3(r)&=\tfrac{3}{2}(r/r_s^3)(r^2-3r_s^2), && r<r_s \\ &=-3, && r>r_s. \end{aligned} \tag{5}$$

The uniform distribution will represent the potential between conduction electrons quite well in the region of large r. It is true that the conduction-electron charge density will have oscillations due to orthogonalization to the cores, but these oscillations will occur within the core region where the other terms $[Z_1(r)$ and $Z_2(r)]$ in the potential predominate. A more important correction arises from the fact that a sum over Wigner-Seitz spheres, as in Eq. (1), does not completely map out the actual crystal. Hence the potential is overemphasized in the region between atoms where the spheres overlap while in other regions which are not enclosed by spheres, the potential is neglected entirely. This can be corrected in the manner first suggested by Heine,[10] and the effect of the correction is included by an additional[14,15] contribution $2Z_5(r)$ to the total $2Z(r)$.

For a heavy metal like indium, the exchange and correlation between conduction electrons is quite difficult to approximate with any reasonable degree of confidence. We have therefore omitted any consideration of these effects in the potential. The various contributions to $Z(r)$ are listed in Table I.

III. OPW CALCULATION AND PSEUDOPOTENTIAL INTERPOLATION

There are a number of excellent reviews[2,10,16] of the theory of the OPW method,[17] so we shall present only a few relevant points of the procedure we have followed.

For the core functions employed in the orthogonalization procedure we used those obtained by solving the Schrödinger equation in the potential $V(r)$ of the conduction electrons and not[10] with the atomic potential. To distinguish between the two, one can refer to the former as quasicore and the latter as atomic-core functions. The quasicore wave functions were found by integrating the Schrödinger equation numerically for the $1s$ through $4d$ wave functions. This was done with the aid of a program originally written by Cooley[18] and modified by Zare and Cashion[19] for use on the IBM 7090.

A general program was written to generate the Hamiltonian matrix H and the overlap matrix S that arise in the variational procedure. For a particular symmetry point and irreducible representation, the various symmetrized wave vectors were initially read in as data and the program calculated the matrix elements of H and S between symmetrized OPW's. To obtain the eigenvalues it is necessary to solve the secular equation $\det|H-ES|=0$. Since some of the properties we are interested in depend on the wave functions, it becomes necessary to solve for the eigenvectors also. Therefore a separate program was written to find S^{-1} and construct the new matrix $H'=S^{-1}H$, and the secular matrix $(H'=EI)$ was then diagonalized.[20]

Following the format outlined above, the energies for the various irreducible representations at the symmetry points were calculated. In Table II, the energies are listed and a comparison is made with the corresponding free-electron energy values.

[13] F. Herman, J. Callaway, and F. S. Acton, Phys. Rev. 95, 371 (1954).

[14] G. D. Gaspari, Ph.D. thesis, University of California, Riverside, 1965 (unpublished).
[15] T. L. Loucks, Ph.D. thesis, Pennsylvanis State University, 1963 (unpublished); T. L. Loucks and P. H. Cutler, Phys. Rev. 133, A819 (1964).
[16] T. O. Woodruff, in *Solid State Physics*, edited by F. Seitz and D. Turnbull (Academic Press Inc., New York, 1957), Vol. 4.
[17] C. Herring, Phys. Rev. 57, 1169 (1940).
[18] J. W. Cooley, Atomic Energy Commission Research and Development Report No. NYO 9490, 1961 (unpublished).
[19] R. N. Zare and R. K. Cashion, University of California Radiation Laboratory Technical Report No. 10881, 1963 (unpublished).
[20] The authors are indebted to Dr. John Fry for the use of a program which diagonalizes a nonsymmetric matrix.

In order to get an idea of the convergence of the energies, it was decided to explicitly test the convergence for several symmetry points. Secular equations as high as 10×10 incorporating up to eighty OPW's were diagonalized. From the results[14] it was felt that errors resulting from truncation of the secular equation would be expected to be less than 0.01 Ry in all cases. It is interesting to note from Table II that the free-electron energies are reasonably close to the OPW values throughout most of the Brillouin zone (BZ). A closer look at the matrix elements $H_{m'm}$ and $S_{m'm}$ indicates the reason for this nearly-free-electron behavior. It was noticed that in $H_{m'm}$ the Fourier coefficients of the crystal potential were being cancelled by the terms from orthogonalization leading to an energy matrix whose diagonal elements were predominantly determined by the kinetic energy, and the off-diagonal elements were considerably smaller than the diagonal elements. This behavior of the Hamiltonian matrix[10,21] forms the basis for the pseudopotential interpolation scheme.[22]

In principle it is possible to use the OPW[15] method to determine the complete band structure; however, the computational effort can be greatly reduced by using the pseudopotential interpolation scheme. A number of alternate procedures[23–27] for the application of the pseudopotential methods to band-structure calculations are available in the literature. To retain the spirit of the first-principle nature of our calculation, we have followed the procedure of using the calculated values of the energy levels at certain symmetry points[27] to determine the pseudopotential parameters rather than utilizing experimental band data for this purpose.

Since our OPW calculation does not employ a **k**-dependent potential, the use of a local pseudopotential is adequate. Here the Fourier coefficient $\langle \mathbf{k}+\mathbf{K}_j | V_p | \mathbf{k} \rangle$ is only a function of the reciprocal lattice vector $\mathbf{K}_j$.

The number of Fourier coefficients of the pseudopotential to be kept as parameters is not well defined but the criterion that they must reproduce the energy values already calculated by the OPW method fairly accurately is sufficient for our purposes. If the parameters do meet this criterion, then we can be confident that the energy bands obtained will be at least as accurate. It was decided to keep only five parameters which are defined by

$$Z_1=V_{000}, \quad Z_2=V_{011}, \quad Z_3=V_{002}, \quad Z_4=V_{110},$$

and

$$V_5=V_K, \tag{6}$$

where **K** is any reciprocal lattice vector whose length is greater than that of (1,1,0). The use of a constant V_K for the higher reciprocal vectors is reasonable since the higher Fourier coefficients are essentially determined by the potential in the core region where V_p is small because of the effective cancellation by orthogonalization. These parameters were determined by solving[14] the five nonlinear simultaneous equations obtained from 2×2 secular equations at the points Σ_1, Δ_1, N_4, X_3', and Z_2'. One could make any choice of the five irreducible representations one uses to obtain the Fourier coefficients but we found that the best over-all fit to the calculated energy values were obtained when the above five representations were used.

The nonlinear simultaneous equations were solved using the Newton-Raphson method[28] and the initial values needed to start the procedure were obtained by perturbation theory. In this way the following values were obtained:

$$Z_1=-0.3603, \quad Z_2=-0.7968\times10^{-2},$$
$$Z_3=-0.9847\times10^{-2}, \quad Z_4=0.2563\times10^{-1}, \tag{7}$$
$$Z_5=0.1494\times10^{-1}.$$

In order to check how well these parameters represented the bands, the energies for a number of irreducible

TABLE II. Energies at points of symmetry from OPW calculations.

Symmetry point	No. of OPW's	OPW energy[a]	Free-electron energy
Γ_1	61	0.0000	0.0000
Γ_3	89	1.640	
Z_2'	80	0.4274	0.4478
Z^1	48	0.4554	
Z_5'	64	0.7107	
Z_3	80	1.0778	
Δ_1	23	0.1209	0.1314
Δ_4	37	1.0869	
X_3'	56	0.4895	0.5255
X_1	44	0.5601	
X_4'	56	0.9264	
X_2'	56	0.9568	
T_3 (doubly degen.)	40	0.5963	0.6375
T_4	44	0.6626	
T_1	44	0.7218	
V_4	38	0.4473	0.4694
V_1	24	0.4891	
V_1	24	0.7886	
U_3	42	0.4673	0.4910
U_1	28	0.5124	
U_4	38	0.7588	
N_1	30	0.3605	0.3747
N_4	30	0.3725	
N_4	30	1.2624	
Σ_1	22	0.1223	0.1336
Σ_4	34	0.8783	
Σ_1	22	0.9400	
S_4	40	0.5114	0.5492
S_1	28	0.6017	
S_3	38	0.6913	

[a] Energies are in rydbergs relative to the bottom of the band.

[21] F. Herman, Phys. Rev. **88**, 1210 (1952); **93**, 1214 (1954).
[22] J. C. Phillips, Phys. Rev. **112**, 685 (1958).
[23] L. Kleinman and J. C. Phillips, Phys. Rev. **116**, 880 (1959).
[24] M. H. Cohen and V. Heine, Phys. Rev. **122**, 1821 (1961).
[25] J. Austin, V. Heine, and L. J. Sham, Phys. Rev. **127**, 276 (1962).
[26] F. Bassani and V. Celli, Nuovo Cimento **11**, 805 (1959); J. Chem. Solids **20**, 64 (1961).
[27] W. A. Harrison, Phys. Rev. **118**, 1182 (1960).
[28] K. Nielson, *Methods in Numerical Analysis* (The MacMillan Co., New York, 1956).

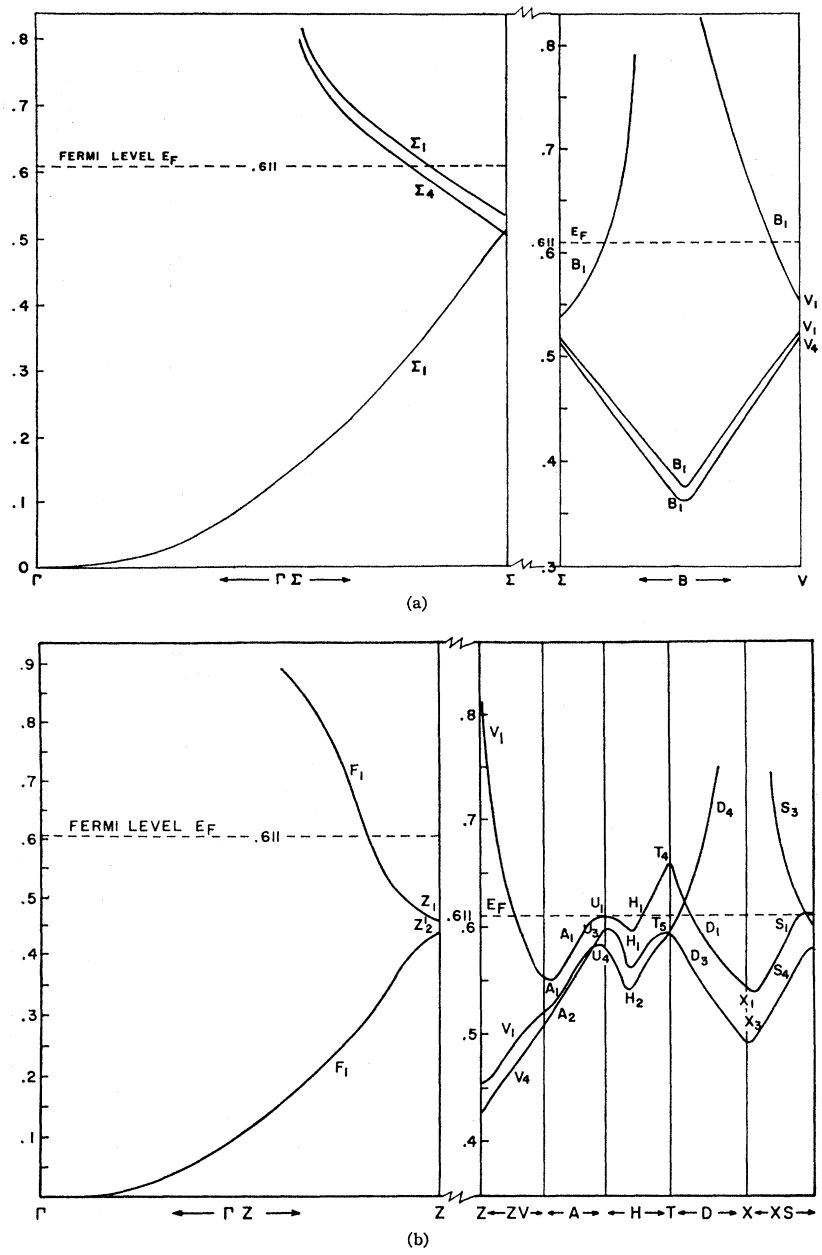

FIG. 2. Calculated energy bands of indium.

representations were computed and compared with the OPW calculation. This comparison is presented in Table III, where the energies are relative to the bottom of the band. The agreement is quite favorable and we can feel confident that the resulting bands will be as accurate.

Using the calculated pseudopotential parameters, the energies along symmetry lines $\Gamma\Sigma$, ΓZ, ZV, ZU, A, B, D, F, and H (Fig. 1) were calculated. For all these cases, a third-order secular equation was used, and the resulting energy bands are shown in Fig. 2. The value of the Fermi energy indicated in the figure was not obtained by a direct calculation but rather by an empirical method. For a direct calculation one has to obtain constant energy surfaces $E_k = E_0$ in k-space and slowly alter E_0 until the volume enclosed by the constant energy surface is equal to $1\frac{1}{2}$ times the volume of the BZ. Since this procedure would require much additional labor and computing time, it was decided to use experimental data to determine the Fermi energy E_F.

It has already been pointed out that the OPW energy values differed slightly (Table II) from the free-electron energies; in fact, the average difference is approximately 0.025 Ry. It seems reasonable to assume that the Fermi energy is somewhat lower than the free-electron value of 0.633 Ry. One could then determine the Fermi

energy by comparing topological features such as the extremal dimensions and areas of the Fermi surface for a number of choices of the Fermi energy in the neighborhood of 0.633 Ry with the experimental results of Rayne and co-workers.[5,6] In order to facilitate such a comparison the nearly-free-electron Fermi surface for the second and third band is reproduced[29] in Figs. 3 and 4. The details of this comparison in terms of the dimensions of the relevant sections of the Fermi surface are described in the next section. It was found that a Fermi energy of 0.611 Ry satisfactorily fitted most of the features of the experimental Fermi surface. The fact that there was no unique Fermi energy, which fitted exactly all the available data, is not very disturbing since certain aspects of the Fermi surface were extremely sensitive to the strength of the potential. Consequently, we had to be satisfied with a Fermi energy

TABLE III. Comparison of energies obtained from pseudopotential and OPW calculations.

Irreducible representation	Pseudopotential energy (Ry)	OPW energy
X_1	0.181[a]	0.210
X_4	0.582[a]	0.576
V_1	0.119[a]	0.139
	0.118[b]	
V_3	0.697[b]	0.703
V_4	0.099[a]	0.097
	0.099[b]	
U_1	0.140[b]	0.162
U_3	0.121[a]	0.117
	0.120	
U_4	0.406[b]	0.409
N_1	0.0064[a]	0.011
T_4	0.315[a]	0.313
T_3	0.252	0.246
Δ_4	0.714[a]	0.736
	0.712[b]	

[a] A second-order secular equation was used.
[b] A third-order secular equation was used.

that reproduced the general shape of the Fermi surface quite well.

IV. BAND-STRUCTURE RESULTS AND COMPARISON WITH EXPERIMENT

Having determined the Fermi energy it now becomes possible to proceed to a filling up of the bands. The first band is found to be completely filled while the fourth band is completely empty. This corroborates the conclusions of Rayne and Chadrasekhar[5] from the interpretation of the magnetoacoustic experiments. Merriam[30] has conjectured from an analysis of lattice parameter and superconducting data from In-Pb and In-Sn solid solutions that the first band of indium contained some holes. However, our calculated first band in Fig. 2 is definitely below the Fermi surface and will be completely filled. The nearly-free-electron model of Harrison[31] predicts pockets of electrons in the fourth band but these are removed by the finite crystal potential.

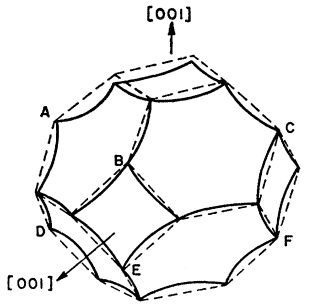

FIG. 3. Free-electron Fermi surface for indium (second band).

The second band surface is found to consist of pockets of electrons around the 14 sides of the polyhedra which extend towards the Γ point. Our calculation indicates that the surface does not make any contact with the BZ boundary, whereas the nearly-free-electron surface (Fig. 3) touches the zone boundary at the corners of the diamond. This behavior is analogous to that found for aluminum by Harrison.[27] If contact were made, there would be a multiply connected surface leading to the possibility of open orbits. Such open orbits have not been observed in the magnetoresistance experiments of Alekseevskii and Gaidukov,[32] lending support to a Fermi surface which is not multiply connected. The anomalous skin effect in indium has been measured by Dheer[33] indicating that the area of the Fermi surface is 93% of the free-electron Fermi surface. This is in agreement with our second-zone surface since a decrease in the surface area would occur if the surface does not touch the zone boundaries.

The central cross sections of the Fermi surface arising from the second band are shown in Figs. 5 and 6. In Table IV, some extremal dimensions of the second-band Fermi surface are listed for two values of the Fermi energy, the free-electron value of 0.633 Ry and the chosen value of 0.611 Ry, and these dimensions are compared with the free-electron model and the experimental results of Rayne.[5] This comparison gives support to the speculation that the second-band Fermi surface

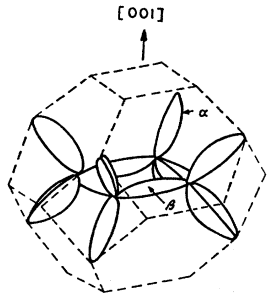

FIG. 4. Free-electron Fermi surface for indium (third band).

[29] The authors are grateful to Dr. J. A. Rayne for Figs. 3–6.
[30] M. F. Merriam, Phys. Rev. Letters **11**, 321 (1963).
[31] W. A. Harrison, Phys. Rev. **116**, 555 (1959).
[32] N. E. Alekseevskii and Yu. P. Gaidukov, Zh. Eksperim. i Teor. Fiz. **36**, 447 (1959) [English transl.: Soviet Phys.—JETP **9**, 311 (1959)].
[33] P. N. Dheer, Proc. Roy. Soc. (London) **A260**, 33 (1961).

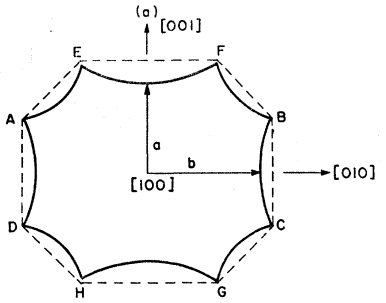

FIG. 5. Cross section of the second-band Fermi surface in a plane perpendicular to [100] direction in the nearly-free-electron approximation.

can be qualitatively described by the nearly-free-electron model.

From Fig. 2, the third-band electrons are seen to be located on and near the symmetry lines A and H. In the nearly-free-electron model, these sections can be pieced together resulting in a surface shown in Fig. 4 centered around the symmetry point Z. Owing to the fact that for indium we are dealing with a tetragonal lattice, the symmetry lines A and H and consequently the two arms α and β are not equivalent as they were for aluminum[31] where the lattice was cubic.

The existence of the β arms is well established experimentally[5,6,34,35] and some of the extremal dimensions and cross sections are available.[5,6] Our calculations [Fig. 2(b)] indicate that these arms are not pinched off at the ends and form a loop[34,35] as expected from the free-electron model. In Tables IV and V the experimental dimensions and cross sections are compared with the results of our calculation for two choices of the Fermi energy and the free-electron model. The choice of 0.611 Ry for the Fermi energy leads to generally good agreement between theory and experiment while the predictions of the free-electron model are significantly larger.

The cyclotron mass of the β arms for a magnetic field in the (110) direction has been determined by Brandt and Rayne[6] from the temperature variation of the de Haas–van Alphen oscillations using the relationship

$$m^*/m_0=(1/\pi)dA/dE, \tag{8}$$

dA/dE being the rate of change of cross-sectional area with energy and m_0 the free-electron mass. The experimental value is found to be $(m^*/m_0)_{\text{exp}}=0.19$. From a graphical analysis of calculated contours around the Fermi energy 0.611 Ry we have obtained a theoretical value of $(m^*/m_0)_{\text{calc}}=0.11$. This discrepancy between the experimental and theoretical cyclotron mass was found to persist for various choices of the Fermi energy. This type of disagreement has been found for aluminum by Harrison[27] and for lead by Anderson and Gold.[36] These authors state that better agreement would be obtained if one were to replace the free-electron mass with a renormalized mass including electron-phonon interactions.

Brandt and Rayne[6] have observed the de Haas–van Alphen oscillations associated with the α arms. On the other hand, Mina and Khaikin,[34] from cyclotron resonance studies, and Gantmakher and Krylov,[35] from (rf) size-effect measurements, failed to detect effects associated with the α arms. Our band-structure results [Fig. 2(b)] for the line H give definite evidence for the existence of the α arms. The results indicate that the α arms are pinched off at the point T but seem to make slight contact with the β arms.

TABLE IV. Comparison of the theoretical and experimental extremal dimensions of the Fermi surface.

Zone	Dimension designation	$(\text{OPW})_1$[a]	$(\text{OPW})_2$[b]	Free electron	Mean experimental[c]
2	a	1.01[d]	1.03	1.04	1.03
	b	1.20	1.24	1.24	1.19
	c	1.07	1.12	1.13	1.03
3	f	0.38	0.36	0.42	0.35
	g	0.32	0.25	0.39	0.25

[a] Using a Fermi energy of 0.633.
[b] Using a Fermi energy of 0.611.
[c] Values obtained from Rayne (Ref. 5).
[d] All units are in Å^{-1}.

V. SPIN-ORBIT EFFECTS

So far we have treated the conduction electrons as nonrelativistic particles but since indium is not a very light metal it is important to calculate the effects of the spin-orbit interaction. In this section we are interested in calculating the magnitude of the spin-orbit interaction for states near the Fermi surface. Those energy levels which have been accurately determined belong to the irreducible representations X_1, S_1, T_5. Of these, T_5 is particularly interesting since it is a doubly degenerate level (not including spin) where the second-band Fermi surface almost touches the zone boundary. Besides, T_5 has no s symmetry but has p and d symmetry, hence we expect it to be a good candidate for the study of spin-orbit interaction for electrons at the Fermi surface.

If spin is included, T_5 is a fourfold-degenerate level and will split into two twofold degenerate levels when spin-orbit effects are considered.[9] That is, the direct product representation of $T_5\times D^{1/2}$ contains the two additional two-dimensional representations T_6 and T_7.

$$T_5\times D^{1/2}=T_6+T_7.$$

From the irreducible representation of T_6 and T_7 one can construct the correct symmetrized combinations of OPW's transforming as particular rows of T_6 and T_7

[34] R. T. Mina and M. S. Khaikin, Zh. Eksperim. i Teor. Fiz. 48, 111 (1965) [English transl.: Soviet Phys.—JETP 21, 75 (1965)].
[35] V. F. Gantmakher and I. P. Krylov, Zh. Eksperim. i Teor. Fiz. 49, 1054 (1965) [English transl.: Soviet Phys.—JETP 22, 734 (1966)].
[36] J. R. Anderson and A. V. Gold, Phys. Rev. 139, A1459 (1965).

and we know that there will then be no mixing between these under spin-orbit interaction.

For T_5 we consider the eight OPW's constructed from the following wave vectors:

$$\begin{aligned}|\mathbf{k}_1\rangle&=(\pi/a,\pi/a,\pi/c),\\ |\mathbf{k}_2\rangle&=(-\pi/a,-\pi/a,\pi/c),\\ |\mathbf{k}_3\rangle&=(\pi/a,-\pi/a,-\pi/c),\\ |\mathbf{k}_4\rangle&=(-\pi/a,\pi/a,-\pi/c),\end{aligned}\tag{9}$$

combined with the spin functions

$$\alpha=\begin{pmatrix}1\\0\end{pmatrix}\quad\text{and}\quad\beta=\begin{pmatrix}0\\1\end{pmatrix}.$$

The correct symmetrized OPW's transforming like different rows of the single group of T_5 are given by

$$\begin{aligned}|a\rangle&=|\mathbf{k}_1\rangle-|\mathbf{k}_2\rangle-|\mathbf{k}_3\rangle+|\mathbf{k}_4\rangle,\\ |b\rangle&=|\mathbf{k}_1\rangle-|\mathbf{k}_2\rangle+|\mathbf{k}_3\rangle-|\mathbf{k}_4\rangle.\end{aligned}\tag{10}$$

One can easily obtain the correct symmetrized combination transforming as T_6 and T_7 by applying the usual projection operator[37] to either $|a\rangle\alpha$ or $|a\rangle\beta$ or similarly $|b\rangle\alpha$ or $|b\rangle\beta$. Following this procedure the symmetrized combination of OPW's transforming like different rows for T_6 and T_7 are

$$\begin{aligned}|c\rangle&=\frac{1}{2\sqrt{2}}[(1-i)|k_1\rangle\beta-(1-i)|k_2\rangle\beta\\ &\qquad-(1+i)|k_3\rangle\beta+(1+i)|k_4\rangle\beta],\\ |c'\rangle&=\frac{1}{2\sqrt{2}}[(1+i)|k_1\rangle\alpha-(1+i)|k_2\rangle\alpha\\ &\qquad-(1-i)|k_3\rangle\alpha+(1-i)|k_4\rangle\alpha],\\ |d\rangle&=\frac{1}{2\sqrt{2}}[(1+i)|k_1\rangle\beta-(1+i)|k_2\rangle\beta\\ &\qquad-(1-i)|k_3\rangle\beta+(1-i)|k_4\rangle\beta],\\ |d'\rangle&=\frac{1}{2\sqrt{2}}[(1-i)|k_1\rangle\alpha-(1-i)|k_2\rangle\alpha\\ &\qquad-(1+i)|k_3\rangle\alpha+(1+i)|k_4\rangle\alpha].\end{aligned}\tag{11}$$

In terms of the wave functions (11) one obtains the following first-order energy differences between T_6 and T_5 representations and between T_7 and T_5:

$$\begin{aligned}\Delta E(T_6)&=E(T_5)-E(T_6)=\langle c|H_{\text{s.o.}}|c\rangle=\langle c'|H_{\text{s.o.}}|c'\rangle,\\ \Delta E(T_7)&=E(T_5)-E(T_7)=\langle d|H_{\text{s.o.}}|d\rangle\\ &=\langle d'|H_{\text{s.o.}}|d'\rangle.\end{aligned}\tag{12}$$

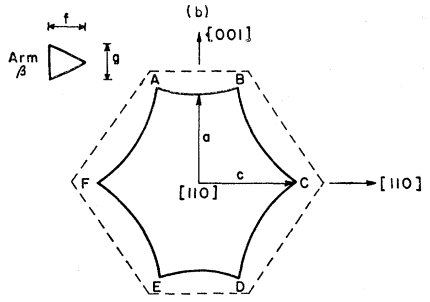

FIG. 6. Cross sections of the second- and third-band Fermi surface in a plane perpendicular to [110] direction in the nearly-free-electron approximation.

These relations for the change in energy due to the spin-orbit interaction are obtained neglecting the admixture of higher levels but since we expect the matrix element connecting the T_6 and T_7 levels to higher levels to be much smaller than the energy separation, this should lead to a rather small correction. We have

$$\Delta E(T_6)=\langle c'|H_{\text{s.o.}}|c'\rangle,\tag{13}$$

where

$$|c'\rangle=\frac{1}{\sqrt{N_{\mathbf{k}}}}(V_{\mathbf{k}}-\sum_c\langle\phi_c|V_{\mathbf{k}}\rangle\phi_c)\alpha\tag{14}$$

and

$$V_{\mathbf{k}}=\frac{1}{\sqrt{N\Omega}}\sum_{q=1}^{4}C_q|\mathbf{k}_q\rangle,$$

where $N_{\mathbf{k}}$ is a normalization constant. The values of C_q are the coefficients for $|c'\rangle$ in Eq. (11). In the matrix element for ΔE there are plane-wave–plane-wave, plane-wave–core, and core-core parts. It has been shown by Cohen and Falicov,[38] and Liu[39] that over 90% of the matrix element comes from the core-core part. On retaining only the core-core part of the matrix ele-

TABLE V. Comparison of extremal cross-sectional areas of the Fermi surface.

Direction of magnetic field	$(\text{OPW})_1$[a]	$(\text{OPW})_2$[b]	Free electron	Exp.[c]
100	0.103[d]	0.067	0.094	0.058
110	0.075	0.042	0.079	0.044

[a] Cross-sectional area of Fermi surface using Fermi energy of 0.633.
[b] Cross-sectional area of Fermi surface using Fermi energy of 0.611.
[c] Brandt and Rayne (Ref. 6).
[d] Units are Å^{-2}.

[37] R. S. Knox and A. Gold, *Symmetry in the Solid State* (W. A. Benjamin, Inc., New York, 1964).

[38] M. H. Cohen and L. M. Falicov, Phys. Rev. Letters **5**, 544 (1960).

[39] L. Liu, Phys. Rev. Letters **6**, 683 (1961).

ment we obtain the following result:

$$\Delta E=\frac{3\pi i}{N_k}\alpha^2\sum_{n=2}^{4}\sum_{n'=2}^{4}B_{n1}(\mathbf{k}_q)B_{n'1}(\mathbf{k}_q)\int R_{n1}R_{n'1}\frac{dV}{dr}rdr$$
$$\times\sum_{q,q'=1}^{4}C_qC_{q'}{}^*\frac{(\mathbf{k}_{q'}\times\mathbf{k}_q)_z}{|k_q|^2}+\frac{12\pi i}{N_k}\alpha^2\sum_{n=3}^{4}\sum_{n'=3}^{4}B_{n2}(\mathbf{k}_q)$$
$$\times B_{n'2}(\mathbf{k}_q)\int R_{n2}R_{n'2}\frac{dV}{dr}rdr\sum C_qC_{q'}{}^*$$
$$\times\frac{(\mathbf{k}_q\cdot\mathbf{k}_{q'})(\mathbf{k}_{q'}\times\mathbf{k}_q)_z}{|k_q|^4}, \quad (15)$$

where

$$B_{n1}(\mathbf{k}_q)=\int j_1(k_qr)R_{n1}r^2dr,$$
$$B_{n2}(\mathbf{k}_q)=\int j_2(k_qr)R_{n2}r^2dr, \quad (16)$$

and R_{n1} and R_{n2} are radial p and d core wave functions with principal quantum number n. The first part of the right-hand side is the p contribution and the second part is the d contribution. Making use of the C_q from Eq. (11) and performing the necessary computations using our calculated potential (Table I), the following results are obtained:

$$\Delta E(T_6)=0.0131\text{ Ry},$$
$$\Delta E(T_7)=-0.0131\text{ Ry}, \quad (17)$$

and a splitting $E_{T_6}-E_{T_7}=0.0262$ Ry. As expected, the spin-orbit effect is larger in magnitude than for magnesium[38] but is still rather small. This relatively small effect of the spin-orbit interaction in indium metal can be understood by realizing that the spin-orbit Hamiltonian is effective mainly over the core region which is a small fraction of the atomic cell due to the nearly-free-electron behavior of the conduction electrons.

If we assume that spin-orbit effect does not change the Fermi energy, the T_6 level will lie just below the Fermi surface indicating that the second-band Fermi surface still does not touch the zone boundary. It should be remembered, however, that the band structure is only accurate to 0.01 Ry, and since spin-orbit effects are of this order of magnitude, a more detailed investigation over the entire Fermi surface does not seem warranted.

VI. KNIGHT SHIFT

The expression for the Knight shift in a magnetic field can be shown to be[40]

$$\Delta H/H=(8\pi/3)\chi_p\langle|\psi_k(0)|^2\rangle_{av}, \quad (18)$$

where χ_p is the Pauli paramagnetic susceptibility per atom and $\langle|\psi_k(0)|^2\rangle_{av}$ is the density at the nucleus due to a conduction electron averaged over the Fermi surface.

In order to calculate the Knight shift for indium, a knowledge of χ_p is necessary. Since no electron-spin-resonance experiments have been performed on indium, χ_p was obtained from the low-temperature specific-heat data of Bryant and Keesom,[41] the relation being[40]

$$\chi_p=3(\mu_B/\pi k)\gamma, \quad (19)$$

where the specific heat $C_v=\gamma T$ at low temperature, μ_B is the Bohr magneton, and k is the Boltzmann constant. It should be noted that Eq. (19) applies rigorously to a system of noninteracting electrons. In a real metal, one expects χ_p to be increased above the free-electron value because of exchange effects, since adding electrons of parallel spin increases the exchange energy. But it is also true that the correlation energy between electrons of antiparallel spin is reduced when the spins align themselves, which would lead to a reduction in χ_p. From the calculations of Bohm and Pines,[42] χ_p for free electrons appears to increase somewhat when electron-electron interactions are taken into account. In line with our neglect of the effects of exchange and correlation on band structure and because of the uncertainty of the importance of this correction for Bloch electrons, we have not included the effects of correlation on χ_p.

Bryant and Keesom[41] have determined γ for indium from their specific-heat measurements. They obtain a value of

$$\gamma=1.4035\times10^2\text{ erg/g at. deg}^2. \quad (20)$$

Substituting this value into (42) gives for χ_p

$$\chi_p=1.403\times10^{-6}\text{ volume units}. \quad (21)$$

The remaining quantity that needs to be evaluated is:

$$\langle|\psi_k(0)|^2\rangle_{av}=\frac{\int|\psi_k(0)|^2|\nabla_kE|^{-1}dA_F}{\int|\nabla_kE|^{-1}dA_F}, \quad (22)$$

where the integration is over the area of Fermi surface.

For wave functions built out of OPW's the integral in Eq. (22) is extremely difficult to evaluate since no simple analytic expressions are available for the variation of OPW's with the wave vector $\mathbf{k}$. In order to get an approximate answer it was necessary to replace the integral in (22) by a sum which was then evaluated at a few representative points on the Fermi surface. Since the third band contains a rather small fraction of the conduction electrons, it was assumed that most of the electrons contributing to the Knight shift were in the second band. Assuming this, we then evaluated $\psi_k(0)$

[40] W. D. Knight, in *Solid State Physics*, edited by F. Seitz and D. Turnbull (Academic Press Inc., New York, 1957), Vol. 2.

[41] C. A. Bryant and P. H. Keesom, Phys. Rev. Letters 4, 460 (1960).

[42] D. Pines, in *Solid State Physics*, edited by F. Seitz and D. Turnbull (Academic Press Inc., New York, 1955), Vol. 1.

and $\nabla_k E$ at three points on the second-zone Fermi surface (along $\Gamma\Delta$, ΓZ, and ΓN) and averaged the results. The procedure yields

$$\langle|\psi_k(0)|^2\rangle_{av}=691.01\,, \tag{23}$$

leading to a Knight shift of

$$\sigma_{theor}=(\Delta H/H)_{theor}=0.81\%\,. \tag{24}$$

Recent experiments[8] on the Knight shift in indium at 4.2°K gives

$$\sigma_{exp}=(\Delta H/H)_{exp}=0.82\%\,, \tag{25}$$

in good agreement with earlier results[7] at room temperature.

The qualitative significance of the extremely good agreement between our theoretical value of the Knight shift and experiment is difficult to assess because we have not taken into account two other important sources that could contribute to the Knight shift. One of these is the orbital contribution to the Knight shift which would be of the Landau type[43] or the Van Vleck-Ramsey type.[44] Both of these types of contributions are expected to be small because of the nearly-free-electron behavior of the conduction electrons in indium. The Landau-type contribution is expected to be small because the effective mass is not very different from the free-electron mass. The Van Vleck-Ramsey contribution is also expected to be small because for nearly-free-electron behavior, there would not be much angular momentum of the conduction electrons with respect to the nucleus as origin. The other important source is the core-polarization effect.[45,46] It is a little difficult to speculate on the importance of this effect without actual calculation. However, the good agreement with the direct contribution to the Knight shift and experiment might indicate that the core-polarization effect does not contribute very much to the Knight shift in indium. This belief is further reinforced by recent relaxation-time measurements[47] which indicate good agreement between T_1 and σ_{exp} (and σ_{theor}) in terms of the Korringa relation.[48]

VII. CONCLUSION

We have obtained the band structure of indium using a potential which contains all contributions except correlation and exchange between conduction electrons and the OPW method combined with the pseudopotential interpolation scheme. From these energy bands we are able to interpret fairly satisfactorily a number of detailed features of the Fermi surface which have been observed experimentally. Spin-orbit effects have been analyzed and are shown to be relatively ineffective in influencing the band structure. The wave functions at the Fermi surface obtained in this calculation lead to an isotropic Knight shift in satisfactory agreement with experiment. Two other properties which are currently available for indium and which could be used as a test of the accuracy of the wave functions and the model adopted are the anisotropic Knight shift and the nuclear quadrupole coupling constant.[7,8] However, an evaluation of these properties will have to await accurate methods of interpolating wave functions in **k** space because they require for their interpretation careful integrations throughout the Fermi volume and over the Fermi surface.

For more accurate calculations in the future, it would be instructive to consider d hybridization of the conduction electrons, instead of assuming the d electrons to be localized core electrons. Finally, correlation and exchange effects between conduction electrons should be taken into account in a consistent manner perhaps following the procedures outlined by Hubbard,[49] and more recently by Kohn and Sham[50] and Hedin.[51]

ACKNOWLEDGMENTS

The authors are grateful to Dr. Wei-Mei Shyu and S. D. Mahanti for valuable suggestions and stimulating discussions.

[43] T. P. Das and E. H. Sondheimer, Phil. Mag. **5**, 529 (1960).
[44] R. Kubo and Y. Obata, J. Phys. Soc. Japan **11**, 547 (1956); Y. Obata, *ibid.* **18**, 1020 (1963); A. M. Clogston, A. C. Gossard, V. Jaccarino, and Y. Yafet, Phys. Rev. Letters **9**, 262 (1962).
[45] M. H. Cohen, D. A. Goodings, and V. Heine, Proc. Phys. Soc. (London) **73**, 811 (1959).
[46] G. D. Gaspari, Wei-Mei Shyu, and T. P. Das, Phys. Rev. **134**, A852 (1964); **141**, 603 (1965); **152**, 270 (1966).
[47] D. E. MacLaughlin and J. Butterworth, Phys. Letters **23**, 291 (1966).
[48] J. Korringa, Physica **16**, 60 (1950).
[49] J. Hubbard, Proc. Roy. Soc. (London) **A244**, 199 (1958).
[50] W. Kohn and L. Sham, Phys. Rev. **145**, 561 (1966).
[51] L. Hedin, Arkiv Fysik **30**, 558 (1965).